

Article

# 2-DOF Woven Tube Plane Surface Soft Actuator Using Extensional Pneumatic Artificial Muscle

Moe Kuriyama \* and Toshio Takayama 

Department of Mechanical Engineering, Tokyo Institute of Technology, 2-12-1, Ookayama, Tokyo 152-8550, Japan; takayama.t.aa@m.titech.ac.jp

\* Correspondence: kuriyama.m.aa@m.titech.ac.jp; Tel.: +81-3-5734-2820

**Abstract:** Soft actuators, designed for fragile item conveyance and navigation in complex environments, have garnered recent attention. This study proposes a cost-effective soft actuator, created by weaving tubes into twill patterns, capable of transportation and movement. The actuator achieves this by inducing traveling waves on its upper and lower surfaces through sequential pressurization of tubes. Notably, its fabrication does not require specialized molds, contributing to cost efficiency. The single actuator generates traveling waves with two degrees of freedom. Conventional silicone tube-based actuators demonstrate slow transport speeds (3.5 mm/s). To address this, this study replaced silicone tubes with pneumatic artificial muscles, enhancing overall body deformation and actuator speed. Experiments involving both extensional and contractional artificial muscles demonstrated that soft actuators with extensional artificial muscles significantly improved transportation and movement speed to 8.0 mm/s.

**Keywords:** soft robotics; PAMs; traveling wave

## 1. Introduction

Belt conveyors are typical transportation machines that are widely used in various industries. However, these devices typically offer one degree of freedom (DOF) in their transportation direction. To enable 2-DOF transportation, some conveying systems use omnidirectional wheels within the conveying area [1,2] or incorporate omnidirectional driving gears [3] instead of belts. Omnia Wheel Ltd. (Beresfield, Australia) [1] developed a conveying device with omnidirectional wheels placed in a grid pattern for logistics and manufacturing purposes. Zaher et al. [2] presented a path-planning method, employing reinforcement learning, to enhance transportation speed with a conveyor using omnidirectional wheels in a triangular grid pattern than conventional methods. Abe et al. [3] developed an omnidirectional transport table using units with omnidirectional drive gears driven by spur gears positioned in two orthogonal directions. However, machines employing omnidirectional wheels or gears may not be suitable for fragile items, as they tend to cause damage to the transported objects.

Various approaches have been proposed for addressing this issue, employing various technologies such as air jets [4,5], magnetic forces [6,7], ultrasonic technologies [8,9], and soft actuators. Guelpa et al. [4] introduced a modular conveyor designed for thin wafers in the photovoltaic industry, utilizing air jets to lift and push objects. Zhang et al. [6] developed a magnetic levitation system, providing 6-DOF and contactless operation of magnetized objects, promising swift and precise manipulations. Li et al. [8] created a 2-DOF noncontact platform using near-field acoustic levitation. This platform enables 2-DOF transportation by vibrating two rails placed orthogonally using ultrasonic oscillators.

An example of the use of soft actuators for transportation is a modular conveyor that employs pneumatic bellows designed for transportation and sorting [10]. The conveyor controls the height of each point by pressurizing the bellows, allowing them to transport spherical objects by rolling them. Deng et al. [11] manufactured a soft machine table based



**Citation:** Kuriyama, M.; Takayama, T. 2-DOF Woven Tube Plane Surface Soft Actuator Using Extensional Pneumatic Artificial Muscle. *Hardware* **2024**, *2*, 50–65. <https://doi.org/10.3390/hardware2010003>

Academic Editor: Peter C. Hauser

Received: 22 December 2023

Revised: 20 February 2024

Accepted: 23 February 2024

Published: 4 March 2024



**Copyright:** © 2024 by the authors. Licensee MDPI, Basel, Switzerland. This article is an open access article distributed under the terms and conditions of the Creative Commons Attribution (CC BY) license (<https://creativecommons.org/licenses/by/4.0/>).

on the crawling motion of caterpillars. By controlling the 25 soft actuators on the table, the objects placed on the table can be conveyed and rotated. Jang et al. [12] designed an actuator by using dielectric elastomer balloons. They can generate traveling waves using a small power source. Watanabe et al. [13] developed a soft actuator by thermally welding polyurethane sheets. This actuator enables 2-DOF transportation using only six air valves. Zhao et al. [14] created a device using monolithic soft artificial muscles to transport objects by deforming the surface into various waveforms. By altering the shape of the generated waves, it can transport objects in various trajectories. Soft actuators designed for transportation are expected to be used not only for transporting fragile items but also for carrying the human body [15].

These soft actuators can transport objects by generating traveling waves on the actuator surface and transmitting them to the transported objects. By transmitting these waves to the ground surface of the actuators, they can move along the ground. For example, soft robots can move by generating traveling waves like snails [16,17]. Takeyama et al. [16] and Xin et al. [17] fabricated soft robots that move by sequentially depressurizing air chambers to generate longitudinal waves, for the purpose of moving walls and inspecting inside the gastrointestinal tract, respectively. Soft actuators inspired by various animals, such as iguanas [18], annelids [19], and *Drosophila* larvae [20], also have the capability to move. Soft actuators designed for movement are suitable for carrying human bodies or fragile items [21] and moving in complex environments [22,23]. These robots can be used in nursing care and as exploratory robots. For example, Watanabe et al. [21] created a soft-sheet actuator inspired by the gastropod's locomotion. The soft actuator is designed to move on beds or tatami mats, safely transporting the human body. Xu et al. [22] developed a soft robot with dielectric elastomer actuators, mimicking the locomotion of annelids. This robot, with inherent softness, can adapt to unpredictable environments where conventional rigid robots may fail. Liu et al. [23] presented a modular soft robot inspired by inchworms and snakes. This robot also aims for movement in complex environments.

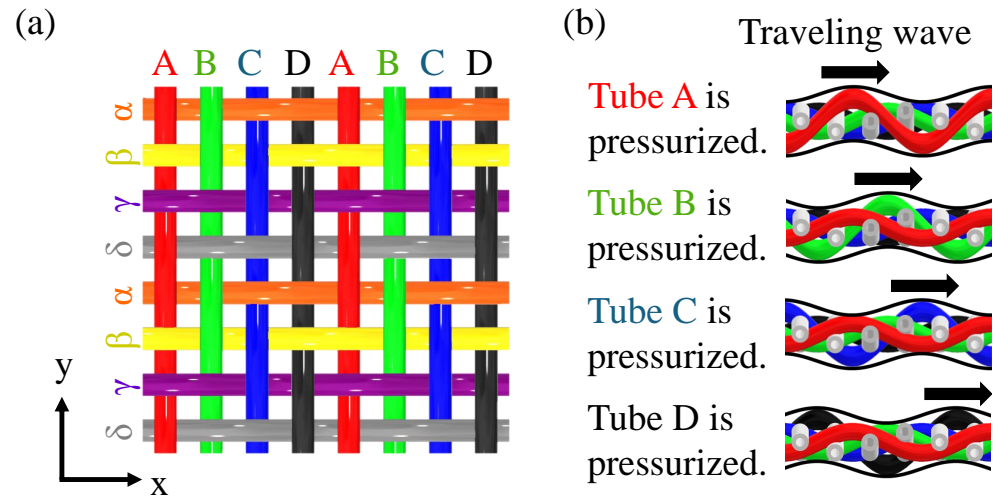
In the present work, we propose a 2-DOF woven-tube plane-surface soft actuator designed for transportation and mobility, offering two distinct advantages. First, it is simple to fabricate. Several soft actuators require specialized molds for fabrication [24,25] and some require complex procedures [26]. For example, the soft robot inspired by the earthworm developed by Ge et al. [26] is created by casting liquid silicone using molds to fabricate various components of the soft robot, and assembling them together. Conversely, the proposed soft actuator can be created by weaving tubes with good pressure deformability without the need for specialized molds. It is easy to fabricate larger or smaller actuators at a low cost. The second advantage is that a single actuator can generate 2-DOF traveling waves. Some soft actuators can only generate 1-DOF traveling waves using a single actuator [27–29]. Hence, it is crucial to use two or more actuators for 2-DOF motions [12,21,26]. For example, the soft sheet actuator developed by Watanabe et al. [21] achieves 2-DOF movements by connecting two actuators in parallel using urethane rods and controlling them. However, our soft actuator can produce 2-DOF traveling waves with a single device and is easy to control and miniaturize.

In a previous study, we proposed the structure of a 2-DOF woven-tube plane-surface soft actuator, employing silicone tubes to achieve faster transportation and movement speeds [30]. However, the optimal transportation speed was slow at 3.5 mm/s. This study aimed to improve the transportation and movement speed of our soft actuator by replacing the silicone tubes with pneumatic artificial muscles (PAMs).

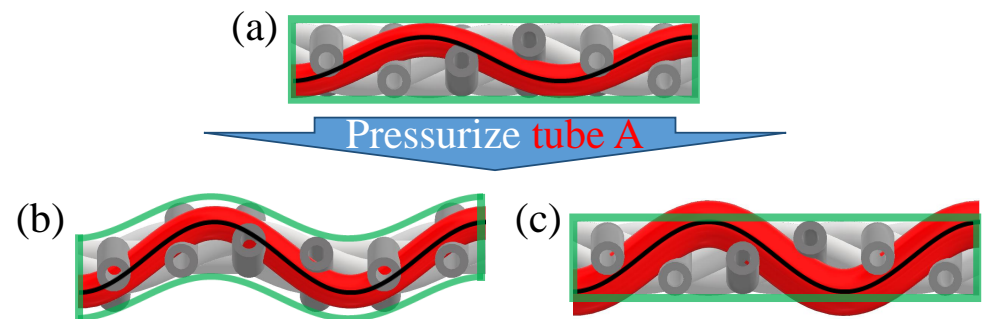
## 2. Design and Methods

Figure 1 demonstrates the 2-DOF woven-tube plane-surface soft actuator. In Figure 1a, the actuator is fabricated by weaving silicone tubes in a 2/2 twill pattern and bonding them. By sequentially applying air pressure to either the vertical or horizontal tubes, it generated traveling waves on its upper and lower surfaces as depicted in Figure 1b. Beginning from the pre-pressurized state in Figure 2a, our initial hypothesis involved the following steps:

the pressurized silicone tubes extended, causing deformations and subsequent movement of the tubes bonded to them. Therefore, the entire body deforms, and traveling waves propagate throughout the actuator as shown in Figure 2b. However, when the cause of the slow transportation speed was investigated, an increase in diameter and length was observed in the pressurized silicone tubes. Consequently, as shown in Figure 2c, only the pressurized tubes deform and generate traveling waves. The difference between the hypothesis and the actual result was deemed the cause of the slow speed.



**Figure 1.** The 2-DOF woven-tube plane-surface soft actuator, where (a) shows the structure of the actuator and (b) shows how to generate traveling waves in the negative direction of the y-axis as shown by the black arrows, respectively.



**Figure 2.** Side view of the 2-DOF woven-tube plane-surface soft actuator, where (a) shows the actuator before pressurizing tube A, (b) shows the expected deformation, and (c) shows the actual deformation, respectively.

We consider why the actuator cannot deform or generate traveling waves throughout the body. Specifically, in the structure shown in Figure 3a, the deformations of the pressurized tubes and the forces applied to the surrounding tubes are considered. Pressurized tubes can deform in four primary ways: decreasing the diameter, increasing the diameter, becoming longer, or becoming shorter. For each type of deformation, the forces applied to the surrounding tubes were analyzed. First, when the diameters of the tubes decreased, as shown in Figure 3b, the tubes originally placed above/below the pressurized tubes were pulled downward/upward.

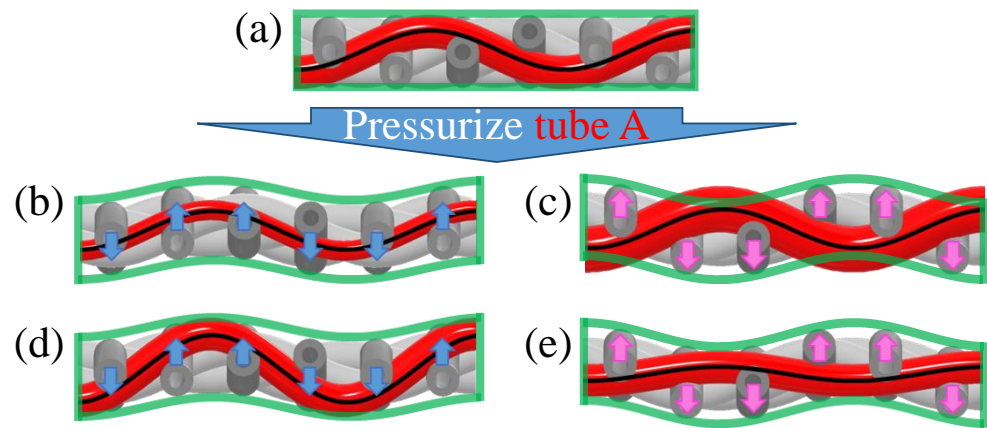


**Figure 3.** Relationship between pressurized tubes deformations and overall body deformations, where (a) shows actuator before pressurizing tube A, (b) shows deformation when tube A decreases diameter, (c) shows when tube A increases diameter, (d) shows when tube A gets longer, and (e) shows when tube A gets shorter, respectively.

Conversely, when the diameters of the tubes increased, as shown in Figure 3c, the forces acted in the opposite direction. Tubes originally placed above/below the pressurized tubes were pushed further upward/downward. Subsequently, when the tubes became longer, as shown in Figure 3d, the surrounding tubes moved in the same manner as in the case of a decrease in diameter. Conversely, when the tubes became shorter, as shown in Figure 3e, the surrounding tubes moved in the same manner as in the case of an increase in diameter. Hence, when the diameters of the pressurized tubes increased and the tubes became longer, the two types of generated force acted in opposite directions, canceling each other. When the actuator with the silicone tubes, which deform as shown in Figure 4a, was pressurized, the diameter increased and the tubes became longer, and the surrounding tubes did not move. In Figure 4, the orange arrows depict the expansion, while the green arrows indicate contraction.

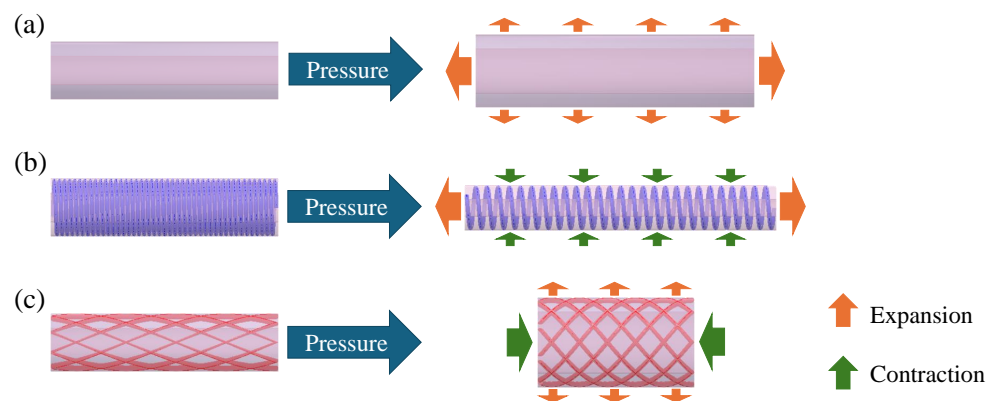


**Figure 4.** Pressurized tube deformation, where (a) shows the silicone tube, (b) shows the extensional PAM, and (c) shows the contractional PAM, respectively.

Therefore, in this study, actuators were fabricated using PAMs instead of silicone tubes. Two types of PAM were utilized: an extensional PAM that decreases in diameter and becomes longer under pressure, and a contractional PAM that increases in diameter and becomes shorter under pressure. The extensional PAM was fabricated by winding a thread around a silicone tube and coating it with silicone. During pressurization, the thread itself does not stretch in the lengthwise direction; thus, the PAM decreases in diameter and increases in length as shown in Figure 4b. The contractional PAM was fabricated by covering a silicone tube with a nylon mesh tube, pulling the mesh tube axially from its

natural length, and then coating it with silicone. During pressurization, the mesh tube tended to return to its natural length; thus, the PAM expanded radially, causing axial contraction and making the tube shorter but wider as shown in Figure 4c. Using these extensional and contractional PAMs, we aimed to deform our actuators throughout the entire body under pressure and improve transportation and movement speeds.

### 3. Build and Operating Instructions

First, we describe the methods used to fabricate PAMs. In this study, PAMs were prepared using commercially available two-component soft silicone, X-32-2428-4 (Shin-Etsu Chemical Co., Ltd., Tokyo, Japan). The manufacturing procedure for the extensional PAM with an inner diameter of 2.5 mm, outer diameter of 5 mm, and length of 250 mm is shown in Figure 5 and is as follows:

1. Commercially available silicone tubes with an inner diameter of 2.5 mm, an outer diameter of 4 mm, and a length of approximately 20 mm were attached to both ends of a metal rod with a diameter of 2.5 mm and a length of 250 mm. Commercially available silicone tubes were connected to the air pressure sources when pressurizing an actuator.
2. In Figure 5a, the metal rod with the attached silicone tubes was placed in one part of the mold designed for tubes with an outer diameter of 4 mm, which consisted of two parts in a set. Well-mixed two-component silicone was poured into both parts of the mold.
3. In Figure 5b, two parts of the mold were assembled, and after 24 h, the hardened silicone was removed from the mold.
4. The metal rod was pulled out from the silicone, and a cotton thread was wound around the silicone.
5. In Figure 5c, a well-mixed two-component silicone was poured into two parts of the mold for the tubes with an outer diameter of 5 mm. From step 4, the silicone tube was placed into one part of the mold.
6. In Figure 5d, the two mold parts were assembled, and after 24 h, an extensional PAM was produced.

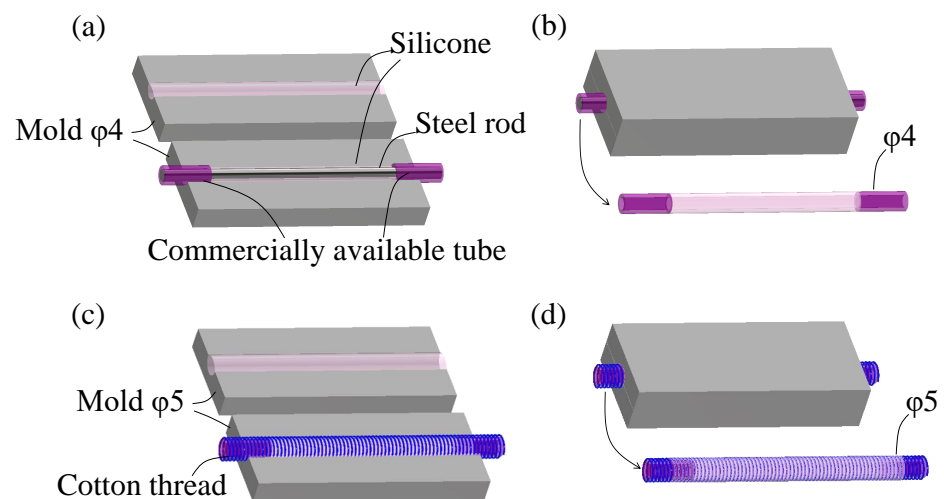


**Figure 5.** Manufacturing procedure of extensional PAM, where (a,b) shows a method for fabricating silicone tube, and (c,d) shows the processing method for extensional PAM, respectively.

Similarly, the manufacturing procedure for the contractional PAM with an inner diameter of 2.5 mm, outer diameter of 6 mm, and length of 250 mm is shown in Figure 6 and is as follows:

1. Shown in Figure 6a, a silicone tube was created in the same way to fabricate the extensional PAM (Steps 1–3).
2. Shown in Figure 6b, the silicone tube was covered with a nylon mesh tube and pulled axially from its natural length.
3. A contractional PAM with an outer diameter of 5 mm was produced in the same way to fabricate the extensional PAM (Steps 5 and 6) as shown in Figure 6c.
4. Using a mold designed for tubes with an outer diameter of 6 mm, an additional silicone layer was created on the outer side in the same way to fabricate the extensional PAM (Steps 5 and 6) as shown in Figure 6d.
5. Finally, the metal rod was removed from the contractional PAM.

To weave the tubes evenly, we utilized threads and jigs in our method as illustrated in Figure 7. The weaving procedure for constructing the actuator is outlined below:

1. Diagonally weave threads into the jig as shown in Figure 7a.
2. Cut tubes to appropriate lengths. On one side of each tube (approximately 1 cm from the end), seal holes with a well-mixed two-component silicone.
3. Weave the tubes on one side of the jig, passing through the threads (Figure 7b). Ensure that the ends with sealed holes from Step 2 are on the same side.
4. Weave the tubes into the other side of the jig, passing through the threads from Step 1 and the tubes from Step 3 (Figure 7c). During this process, ensure that the ends of the tubes with sealed holes from Step 2 are on the same side.
5. Bond the woven tubes together using silicone.

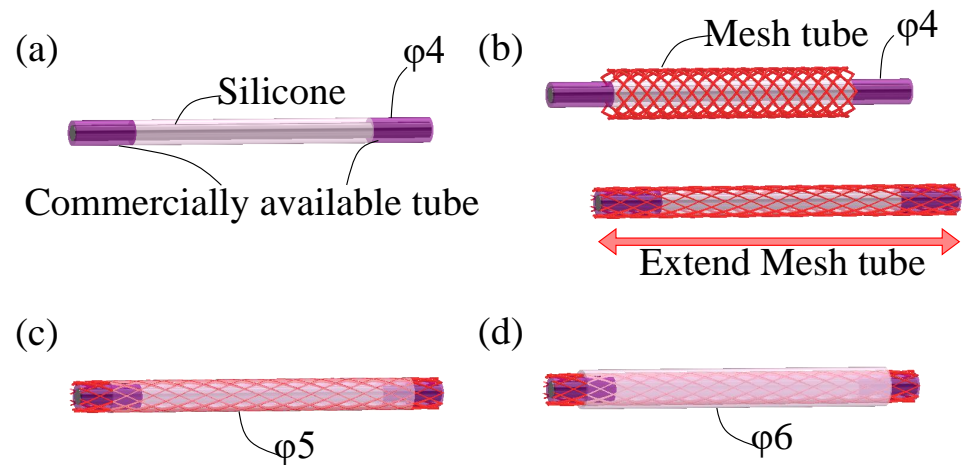


**Figure 6.** Manufacturing procedure of contractional PAMs, where (a) shows the method for fabricating the silicone tube, (b) shows the covering of the silicone tube with a nylon mesh tube, and (c,d) shows the coating of the PAM with silicone, respectively.

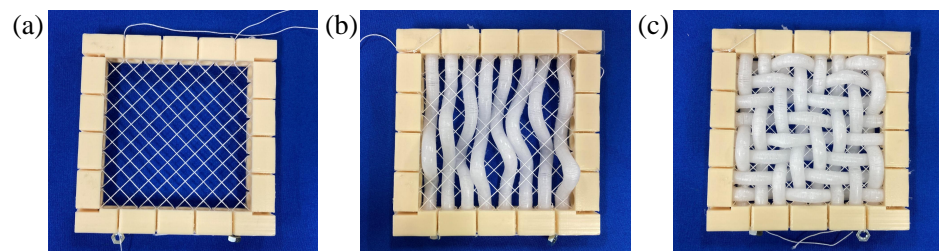


**Figure 7.** Procedure to weave tubes, where (a) shows the threads integrated into a jig, and (b,c) show the extensional PAMs woven inside the jig, respectively.

In this study, molds and jigs were used during the fabrication of PAMs and the weaving process. However, in the future, it will be possible to manufacture this actuator without molds by mechanically weaving commercially produced tubes or PAMs. Furthermore, in the current manufacturing method, the tubes are cut to a length suitable for the actuator size before weaving. Therefore, actuators of various sizes can be easily fabricated.

To conduct transport experiments, we require sufficient space on our actuators because the transported objects move around on them. Therefore, it is necessary to manufacture large actuators. However, it is time-consuming to create large actuators with both extensional and contractional PAMs. Therefore, in this study, small actuators were initially manufactured using both extensional and contractional PAMs. The deformations of these small actuators and their movement speeds were evaluated. Subsequently, by choosing the PAMs that moved faster, a larger actuator was created for the transport experiments.

Two small actuators were fabricated by weaving 16 PAMs (eight vertical and eight horizontal). One uses extensional PAMs and the other uses contractional PAMs. To facilitate weaving, the pitch of the PAMs was set to 8 mm for extension and 10 mm for contraction. The lengths of the PAMs used in the woven area were 70 mm and 90 mm for extension and contraction, respectively. The two actuators are illustrated in Figure 8. The actuator with extensional PAMs weighed 33 g, whereas that with contractional PAMs weighed 52 g.

When these actuators were used, changes in their thicknesses under pressure were measured. We used a laser displacement sensor (CD22-35VM12, OPTEX FA Co., Ltd., Kyoto, Japan) and shone a laser beam onto the actuators for measurement. During pressurization, the height of the actuator at a specific point was measured, and the minimum value was set as the origin. The method for measuring the thickness of the actuator is illustrated in Figure 9a.

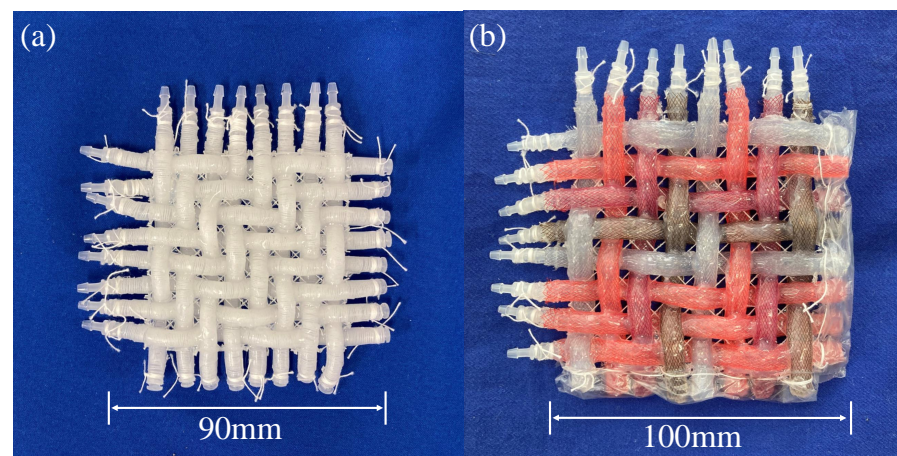


**Figure 8.** Actuators with 16 PAMs (eight vertical and eight horizontal), where (a) shows an actuator with extensional PAMs, and (b) shows an actuator with contractional PAMs, respectively.

In this study, the actuators were powered by applying air pressure. Up to eight solenoid valves (VP544R-6M1-A; SMC Co., Ltd., Tokyo, Japan) driven by a microcontroller board (Elegoo Uno; Elegoo Inc., Shenzhen, China) were used in this study. Considering that the PAMs did not rupture in the pre-experiment, the air pressure applied to the actuator was set at 0.2 MPa (gauge pressure). The pressurization cycle was 600 ms, and each PAM was pressurized for 225 ms. The pressurization sequence of the PAMs is shown in Figure 10. In addition, for comparison with a conventional actuator, the change in the thickness of the actuator using silicone tubes was measured. These silicon tubes had an inner diameter of 1.5 mm and an outer diameter of 6 mm. The actuator was fabricated by weaving 32 tubes (16 vertical and 16 horizontal) with a pitch of 8 mm and tube length of 155 mm in the weaving area. It was pressurized at 0.15 MPa, with the same pressurization sequence as the PAMs. The differences in parameters among the prototypes using the extensional PAM, contractional PAM, and silicone tube are shown in Table 1.

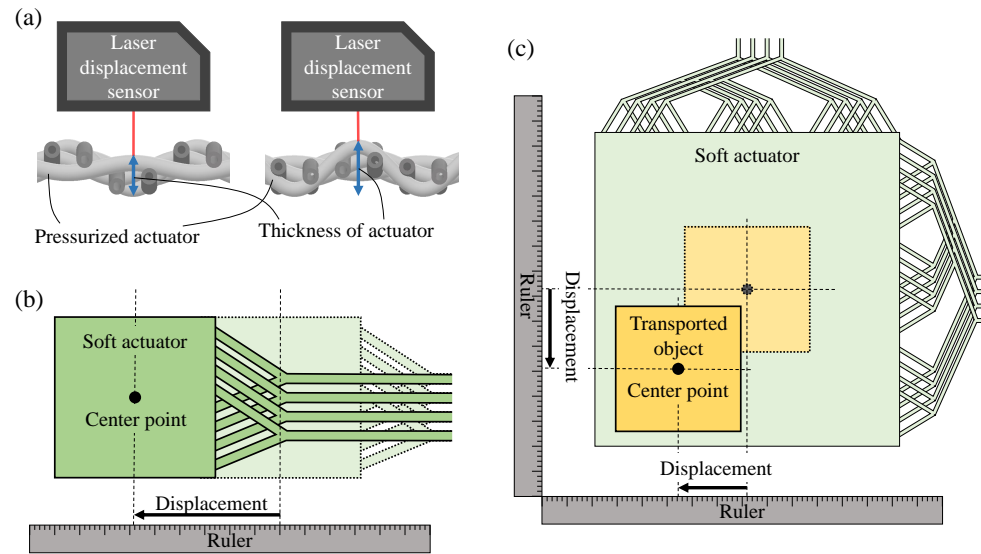


**Figure 9.** Experimental measurement methods, where (a) shows changes in the thickness of an actuator, indicated by the blue arrows, (b) shows the movement speed of an actuator, with the displacement of the actuator represented by the black arrows, and (c) shows the transportation speed of a transported object, with the displacements of the object represented by the black arrows, respectively.

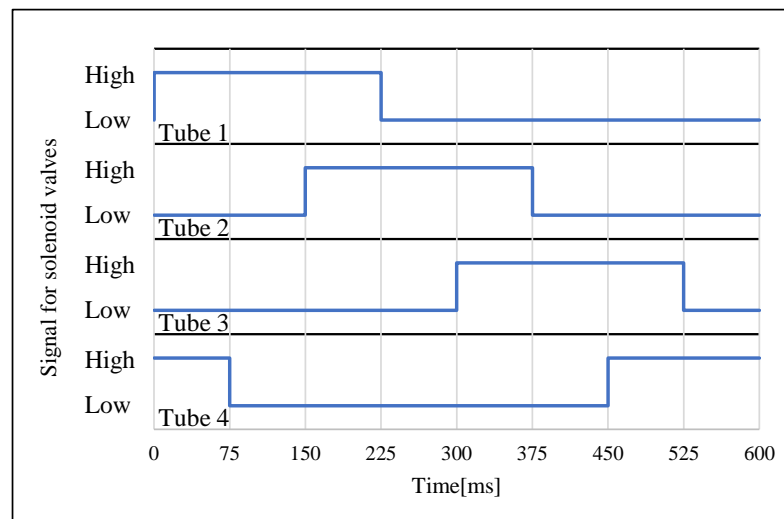


**Figure 10.** Pressurization sequence of PAMs.

**Table 1.** Parameters of various prototypes.

	New Prototype 1	New Prototype 2	Previous Prototype
Types of tube used	Extensional PAM	Contractural PAM	Silicone tube
Inner diameters of tubes used (mm)	2.5	2.5	1.5
Outer diameters of tubes used (mm)	5	6	6
Numbers of tubes in the prototype	16 (eight vertical and eight horizontal)	16 (eight vertical and eight horizontal)	32 (16 vertical and 16 horizontal)
Pitches of tubes in the prototype (mm)	8	10	8
Tube lengths in the weaving area (mm)	70	90	155
Pressures applied to the prototype (MPa)	0.2	0.2	0.15

Subsequently, movement experiments were conducted using two small actuators with PAMs. The actuators were then moved to the flat tables. The actuator was placed on the table, and a ruler was positioned parallel to its direction of movement. The actuator was pressurized, and the movement was recorded in a video. In the video, the central position of the actuator was measured with the ruler at the start of the movement and after 5 s. The displacement of the actuator in the 5 s interval was used to calculate the movement speed. The method for measuring the movement speed is shown in Figure 9b.

Subsequently, a larger actuator with 48 PAMs (24 vertical and 24 horizontal) was fabricated for the transport experiments by selecting the PAMs that moved faster. The transportation speed was measured with a method similar to the measurement of the movement speed. The actuator was positioned on the table. Two rulers, one horizontal and one vertical, were placed parallel to the sides of the actuator. The transported object was placed on the actuator (near the center of the actuator), and the actuator was pressurized. The movement of the object was recorded in a video. In the video, the central position of the transported object was measured with the rulers at the start of transportation and after 5 s. The displacement of the transported object in the 5 s interval was used to calculate the transportation speed. The method for measuring the transportation speed is shown in Figure 9c.

#### 4. Validation

First, the results of the changes in thickness during pressurization of the actuators are shown in Figure 11. The maximum thickness of the actuator using the silicone tubes was approximately 1 mm, whereas for contractional PAMs, it was approximately 2.5 mm, and for extensional PAMs, it was approximately 4 mm. The replacement of silicone tubes with PAMs improved the deformation of the actuator.

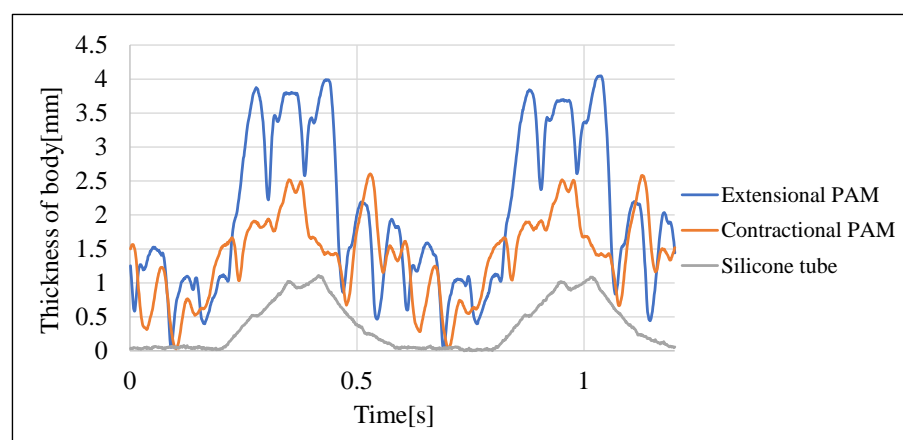


**Figure 11.** Changes in thickness of various soft actuators when they are pressurized.

The results of the movement experiments with small actuators are shown in Figure 12. The actuator with the extensional PAMs moved at 8.0 mm/s, whereas the actuator with the contractional PAMs moved at 6.0 mm/s. They moved approximately 2.3 times and 1.7 times faster than the actuator in the conventional studies, respectively.

Using faster-moving extensional PAMs, we fabricated a larger actuator with 48 PAMs (24 vertical and 24 horizontal) with a pitch of 8 mm and tube length of 210 mm in the weaving area as shown in Figure 13. The weight of the actuator was 258 g. Transport experiments were conducted in the cardinal and diagonal directions, and the transportation velocities are shown in Figure 14. The velocities are expressed using a coordinate system with positive values assigned to rightward and upward directions. During the experiments, the actuator transported a square piece of cardboard with side lengths of 70 mm. The actuator transported the cardboard piece in the cardinal direction, as shown in Figure 15, and the diagonal direction as shown in Figure 16. In these experiments, for transportation

in the cardinal direction, the transportation direction was altered by choosing tubes for pressurizing between the vertical and the horizontal PAMs and reversing the pressurization sequence. For transportation in the diagonal direction, we simultaneously pressurized both the vertical and horizontal PAMs for combining traveling waves in the upward–downward and leftward–rightward directions. To prevent the body of the actuator from moving, the back of the actuator was fixed to the table using packing tape. In the cardinal directions as well as in the upper-left and lower-right directions, the transportation speeds were in the range of 6.9 to 8.0 mm/s, similar to the speed in the movement experiments. However, the speeds for the upper-right and lower-left directions were 5.3 mm/s and 5.1 mm/s, respectively, which were about 65% of the speed in the movement experiments.

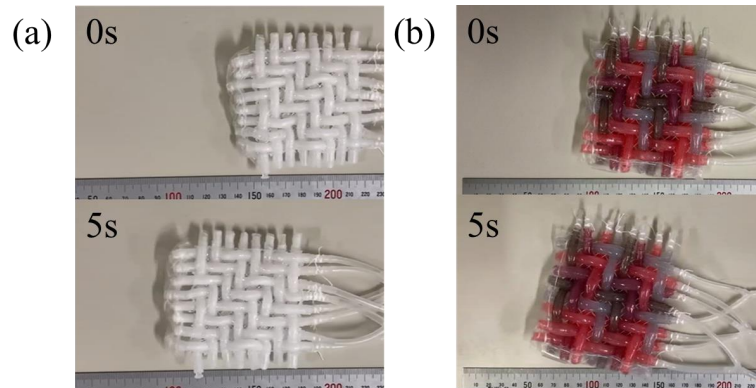


**Figure 12.** Movement experiments, where (a) shows the motion of an actuator with extensional PAMs, and (b) shows the motion of an actuator with contractional PAMs, respectively.

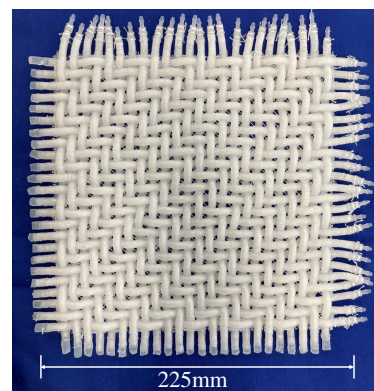


**Figure 13.** Actuator with 48 extensional PAMs (24 vertical and 24 horizontal).

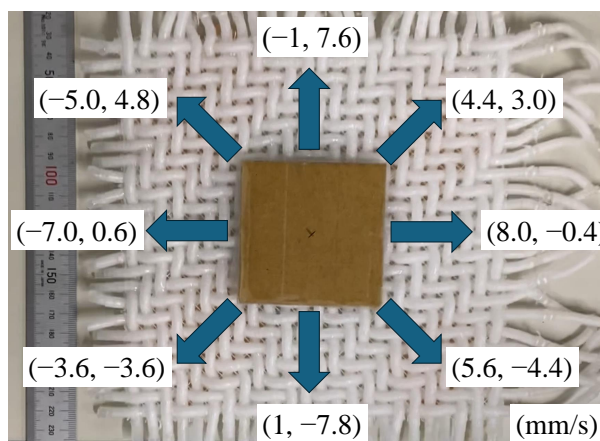


**Figure 14.** Transportation velocities in each direction.

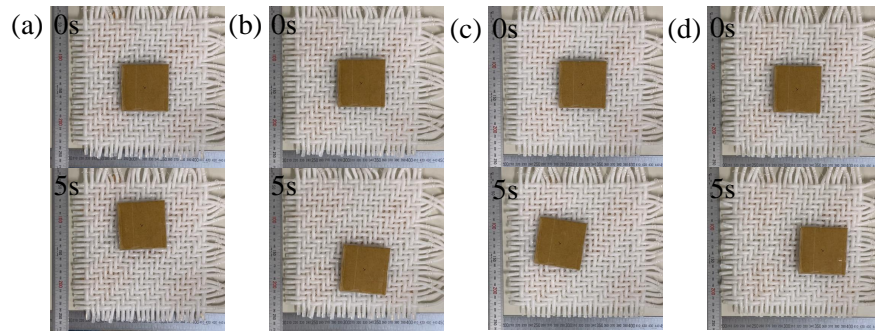


**Figure 15.** Transporting in cardinal directions: (a) upward, (b) downward, (c) leftward, and (d) rightward, respectively.

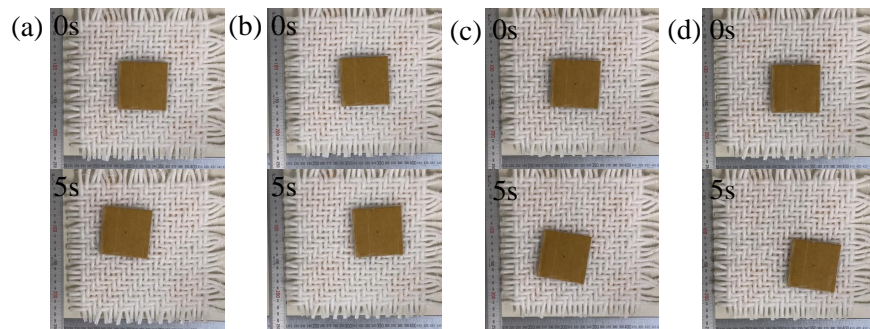


**Figure 16.** Transporting in diagonal directions, where (a) shows an upward-left direction, (b) shows an upward-right direction, (c) shows a downward-left direction, and (d) shows a downward-right direction, respectively.

The adhesion between the back of the actuator and the table was removed, experiments were conducted, where the actuator moved simultaneously with the transportation of the cardboard piece in the cardinal directions. The transport and movement velocities during the experiments are shown in Table 2. The actuator simultaneously transported the cardboard and moved, as shown in Figure 17. Theoretically, during these experiments, the cardboard transport velocity relative to the actuator and the actuator movement velocity relative to the table should be equal and opposite, respectively, making the cardboard appear stationary relative to the table. However, in the experiments, the cardboard was moved at a speed of 2.2–4.6 mm/s relative to the table.

**Table 2.** Transport and movement velocities when the actuator simultaneously transports the cardboard and moves.

	Transporting Direction			
	Upward	Downward	Leftward	Rightward
(i) Transport velocity of the cardboard relative to the desk (mm/s)	(− 0.2, 3.0)	(0.2, −4.6)	(−2.2, 0)	(3.0, 0)
(ii) Movement velocity of the body relative to the desk (mm/s)	(0.2, −5.6)	(−0.7, 5.4)	(5.2, −1)	(−5.9, 1)
(iii) (i)–(ii) Transport velocity of the cardboard relative to the body (mm/s)	(−0.4, 8.6)	(0.9, −10)	(−7.4, 1)	(8.9, −1)

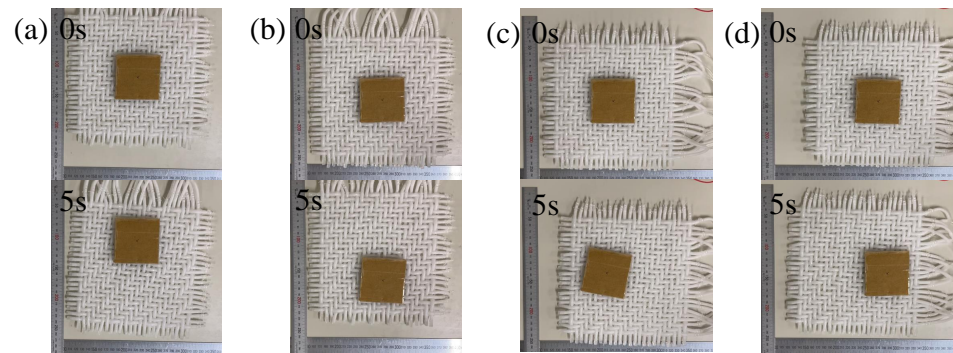


**Figure 17.** Simultaneous transporting and movement, where (a) illustrates upward transporting, (b) demonstrates downward transporting, (c) displays leftward transporting, and (d) illustrates rightward transporting, respectively.

Finally, the actuator was rebonded to the table, and the relationship between the weight of the transported object and the transport speed was investigated. In this experiment, the weight of the transported object was varied in increments of 50 g by adding oil-based clay to a square acrylic plate with side lengths of 70 mm. The experiments were conducted only for downward transportation. The relationship between the weight of the transported object and the transport velocity is illustrated in Table 3 and Figure 18. The transporting angle is represented in a coordinate system, where the right direction is  $0^\circ$ , and the angle increases counterclockwise. When the total weight of the transported object was 50 g, the transport speed was 7.1 mm/s. The transport speed tended to decrease as the total weight of the transported object increased, and at a total weight of 500 g, the transport speed was 5.1 mm/s. Furthermore, a tendency was observed for the transport angle to become larger as the weight of the transported object increased, shifting toward the lower-right direction.

**Table 3.** Relationship between the weight of the transported object and the transportation velocity.

	Weight of Transported Object (g)									
	50	100	150	200	250	300	350	400	450	500
Velocity (mm/s)	(1.1, -7.0)	(1.2, -6.3)	(1.4, -5.9)	(1.5, -5.7)	(1.3, -5.5)	(1.2, -5.3)	(1.2, -5.1)	(1.4, -5.2)	(1.5, -5.2)	(1.5, -4.9)

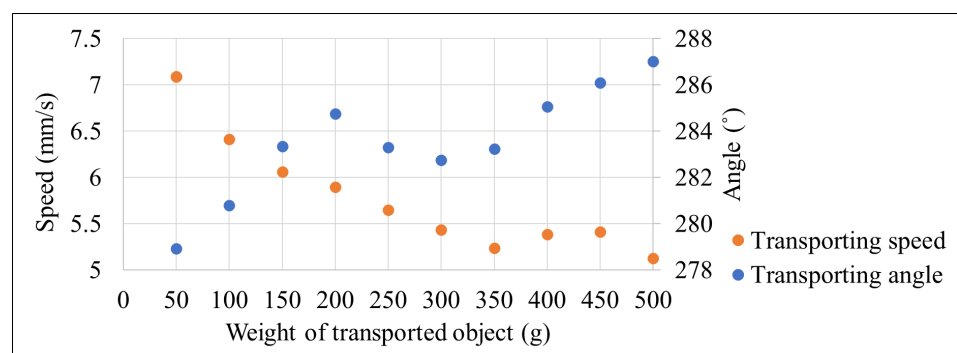


**Figure 18.** Variation in the transport speed and angle with changes in the weight of the transported object.

## 5. Discussion

First, we examined the factors contributing to the greater deformation and faster movement of the actuator using extensional PAMs than the one using contractional PAMs. We focused on the restoration forces of the tubes within the actuator before pressurization, influenced by the weaving patterns of the tubes. As depicted in Figure 19a, these restoration forces act such that for tubes above the center plane, the forces act downward and vice versa. The forces acting on the tubes bonded to the pressurized tube were analyzed considering

the discussion in Section 2. For extensional PAMs, the forces (Figure 19b) aligned with the restoration forces (Figure 19a), facilitating easy deformation under pressure. However, for contractional PAMs, the forces (Figure 19c) opposed the restoration forces, impeding easy deformation. This difference in deformability significantly influences the actuators' deformation and movement speed.

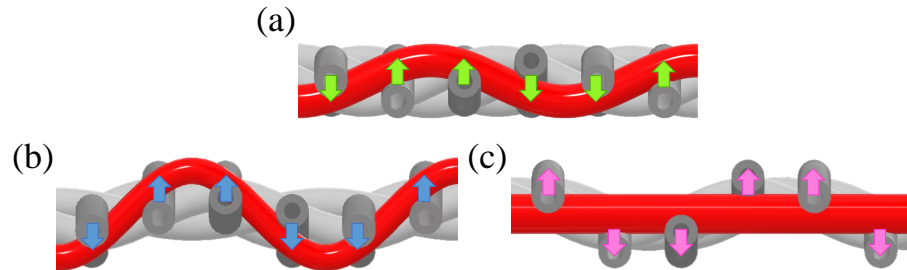


**Figure 19.** Forces in the actuator, where (a) illustrates the restoring forces of the tubes in the actuator before pressurization, (b) reveals the pulling forces acting on the surrounding tubes when the actuator with extensional PAMs is pressurized, and (c) indicates the propelling forces acting on the surrounding tubes when the actuator with contractional PAMs is pressurized, respectively.

Second, the theoretical and measured speeds of the actuator were compared. This actuator is primarily made of silicone rubber, which, because of its high friction coefficient, ideally enables the actuators to move without slipping at the contact points with the ground or the transported object. Based on the ultrasonic motor, which is the typical device driven by traveling waves, the theoretical transportation and movement speed of this actuator was calculated. According to Sugano [31], for the transported object conveyed by the traveling wave of flexural deformation of the elastic body, as shown in Figure 20, assuming no slip at the contact point between the elastic body and the transported object, with the transportation speed of the object as  $U$ , the thickness of the elastic body as  $T$ , the wavelength of the flexural deformation as  $\lambda$ , the amplitude as  $\xi_0$ , and the angular velocity as  $\omega_0$ , Equation (1) is valid:

$$U = -\pi\omega_0\xi_0(T/\lambda) \quad (1)$$

We consider applying Equation (1) to the 2-DOF woven-tube plane-surface soft actuator using extensional PAMs, assuming that the traveling wave in the actuator is ideal and continuous, following a sine wave. Substituting  $T = 14$  mm (the thickness of the actuator),  $\lambda = 8 \times 4 = 32$  mm (considering the pitch of the PAMs, which is 8 mm, and the fact that four PAMs are woven in one cycle),  $\xi_0 = 4/2 = 2$  mm (calculating half of the maximum thickness change, which is 4 mm, as shown in Figure 12), and  $\omega_0 = 2\pi/0.6 \approx 10.5$  rad/s (considering the pressurization cycle period of the actuator, which is 0.6 s) into Equation (1) results in Equation (2) being valid for the transportation and movement speed  $U$  (considering the positive direction as the direction of the traveling wave of the actuator):

$$U \approx -3.14 \times 10.5 \times 2 \times (14/32) \approx -29 \text{ mm/s} \quad (2)$$

However, in reality, because of the periodic motion of the four tubes, the traveling waves become discrete, resulting in an actual speed of 8.0 mm/s, which is 28% of the theoretical speed calculated in Equation (2).

We discuss why the transportation speeds in the upper-right and lower-left directions were slower than those in the other directions. As shown in Figure 14, during upward and leftward transport, the actuator transported the cardboard to the upper-left. In contrast, during downward and rightward transport, the actuator precisely transported it to the lower-right. In other words, the actuator used in the transportation experiments can easily transport it in the upper-left and lower-right directions. For example, when an object is transported to the upper-right, traveling waves for transportation to the upward and rightward directions are combined. However, because the upward transportation is

precisely to the upper-left and the rightward transportation is precisely to the lower-right, they partially cancel each other out in terms of velocity. This is why the transportation speed to the upper-right is slower than that in other directions, which is the same for the lower-left. The specific diagonal directions in which traveling waves are more easily generated by the actuators are determined by weaving the tubes. Two types of stitches appear in twill-weaving patterns: right-leaning and left-leaning. Therefore, the transportation speeds in the diagonal direction were uneven. Theoretically, the speeds in the cardinal directions should be the same. However, in the transport experiments, the speeds varied depending on the transport direction. This variation is believed to stem from slight weaving irregularities in the actuator. This phenomenon could also be attributed to measurement errors.

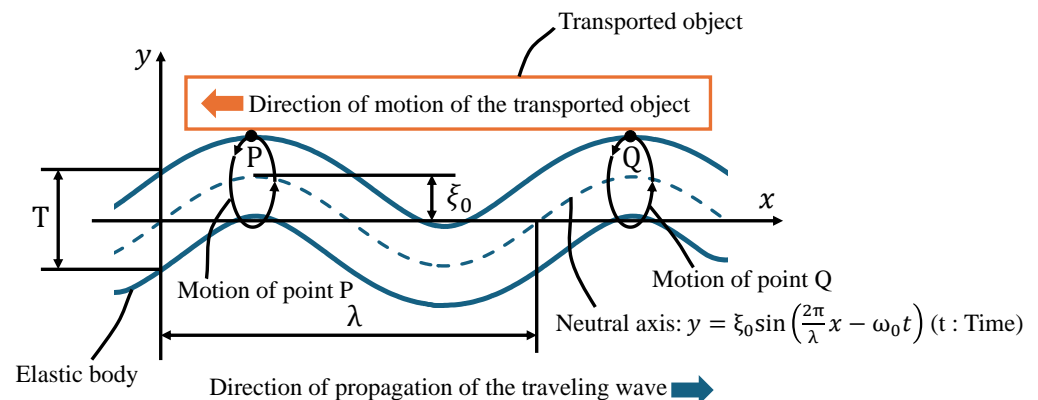


**Figure 20.** Traveling wave of flexural deformation in an elastic body, where the blue solid line represents the elastic body, the blue dashed line indicates the neutral axis of the elastic body, and black circles with arrows illustrate motions of points on the surface of the elastic body.

During simultaneous transportation and movement experiments, the observed motion of the cardboard relative to the table can be elucidated. Focusing on the calculated values of the cardboard transportation speed relative to the actuator, as shown in Table 2, the speeds were in the range of 7.5 to 10 mm/s, which is similar to the speeds in the movement experiments with small actuators. However, the discrepancy arises from the actual movement speeds of the large actuator, weighing 258 g—approximately 7.8 times heavier than the small actuator with extensional PAMs used in movement experiments—which slowed to 5.4–6.0 mm/s. The reason for the decrease in the movement speed as the weight of the actuator increased was the hindrance of the PAMs deformation due to the weight of the body, resulting in smaller overall deformation of the body.

In the transportation experiments where the weight of the transported object was varied, a similar reason can be given for the observed tendency of slower transport speeds with increasing object weight. The deformation of the PAMs was hindered by the weight of the transported object, resulting in smaller deformation of the actuator in the area where the transported object was in contact. During the experiments, the transport speed increased when the weight of the transported object ranged between 350 and 450 g. We attribute this to measurement error.

Finally, the reason for the increase in the transport angle as the weight of the transported object increases, shifting from downward to lower-right direction transport was investigated. This phenomenon is attributed to two factors. First, an increase in the weight of the transported object leads to a slowing of the downward velocity because the deformation of the actuator is hindered by the weight of the transported object, as previously discussed. Second, when the weight of the transported object increases, the rightward velocity does not change significantly, despite some minor errors. However, the reason for this lack of change was not determined in this study. Hence, as the weight of the transported object increased, the downward velocity decreased, and the rightward velocity remained almost unchanged, leading to an increase in the transport angle.

## 6. Conclusions

In this study, we improved the transportation and movement speeds of a 2-DOF woven-tube plane-surface soft actuator by replacing the silicone tubes with PAMs. Regarding movement experiments, two compact actuators were fabricated, each woven with 16 PAMs (eight vertical and eight horizontal). One used extensional PAMs, while the other employed contractional PAMs. The movement speeds achieved were 8.0 mm/s for extensional PAMs and 6.0 mm/s for contractional PAMs, representing approximately 2.3 times and 1.7 times swifter speeds than conventional studies, respectively. Subsequently, employing the extensional PAMs that moved faster, a larger actuator woven with 48 PAMs (24 vertical and 24 horizontal) was fabricated, and transport experiments were conducted. The maximum transport speed reached 8.0 mm/s when the actuator transported a square piece of cardboard to the right side.

This paper experimentally demonstrated the following:

1. By periodically pressurizing woven tubes, 2-DOF woven-tube plane-surface soft actuators can be activated.
2. The use of extensional PAMs for the actuators was effective in efficiently activating them.
3. The actual actuators achieved slower speeds than the theoretical speed because the actual traveling waves in the actuators were discrete, whereas the theoretical speed was calculated under the assumption of continuous traveling waves.

In future studies, we will investigate the speed of our actuators by changing the length and pitch of the PAMs used in the weaving area to achieve faster speeds. We will further advance the performance investigation of the 2-DOF woven-tube plane-surface soft actuators using manufactured prototypes. Simultaneously, we plan to advance generalizations of the performance, such as the speed and propulsion force, in cases where the actuator operates discretely.

**Author Contributions:** Formal analysis, investigation and writing—original draft preparation: M.K.; conceptualization, methodology, formal analysis and writing—review and editing: T.T. All authors have read and agreed to the published version of the manuscript.

**Funding:** This research received no funding.

**Institutional Review Board Statement:** Not applicable.

**Informed Consent Statement:** Not applicable.

**Data Availability Statement:** The datasets used and/or analyzed during the current study are available from the corresponding author on reasonable request.

**Conflicts of Interest:** The authors declare no conflicts of interest.

## Abbreviations

The following abbreviations are used in this manuscript:

DOF	Degree of Freedom
PAM	Pneumatic Artificial Muscle

## References

1. Omni Directional Sortation. Available online: <https://www.omniawheel.com/conveyor-systems> (accessed on 26 October 2023).
2. Zaher, W.; Youssef, A.W.; Shihata, L.A.; Azab, E.; Mashaly, M. Omnidirectional-Wheel Conveyor Path Planning and Sorting Using Reinforcement Learning Algorithms. *IEEE Access* **2022**, *10*, 27945–27959. [CrossRef]
3. Abe, K.; Matsui, G.; Tadakuma, K.; Yamano, M.; Tadakuma, R. Development of the omnidirectional transporting table based on omnidirectional driving gear. *Adv. Robot.* **2020**, *34*, 358–374. [CrossRef]
4. Guelpa, V.; Laurent, G.J.; Dahroug, B.; Le Fort-Piat, N. Modular Contact-Free Conveyors for Handling Planar Fragile Objects. *IEEE Trans. Robot.* **2017**, *33*, 92–101. [CrossRef]
5. Chen, X.; Zhong, W.; Li, C.; Fang, J.; Liu, F. Development of a Contactless Air Conveyor System for Transporting and Positioning Planar Objects. *Micromachines* **2018**, *9*, 487. [CrossRef]

6. Zhang, X.; Trakarnchaiyo, C.; Zhang, H.; Khamesee, M.B. MagTable: A tabletop system for 6-DOF large range and completely contactless operation using magnetic levitation. *Mechatronics* **2021**, *77*, 102600. [CrossRef]
7. Liu, Y.; Sun, X.; Zhao, Z.; Zeng, H.; Chen, W. Stability analysis of near-field acoustic levitation considering misalignment and inclination. *Int. J. Mech. Sci.* **2024**, *265*, 108901. [CrossRef]
8. Li, W.; Zhang, P.; Yang, S.; Cai, S.; Feng, K. A novel two-dimensional non-contact platform based on near-field acoustic levitation. *Int. J. Mech. Sci.* **2024**, *265*, 108865. [CrossRef]
9. Trakarnchaiyo, C.; Wang, Y.; Khamesee, M.B. Design of a Compact Planar Magnetic Levitation System with Wrench–Current Decoupling Enhancement. *Appl. Sci.* **2023**, *13*, 2370. [CrossRef]
10. WaveHandling. Available online: [https://www.festo.com/us/en/e/about-festo/research-and-development/bionic-learning-network/highlights-from-2013-to-2014/wavehandling-id\\_33578/](https://www.festo.com/us/en/e/about-festo/research-and-development/bionic-learning-network/highlights-from-2013-to-2014/wavehandling-id_33578/) (accessed on 23 November 2023).
11. Deng, Z.; Stommel, M.; Xu, W. A Novel Soft Machine Table for Manipulation of Delicate Objects Inspired by Caterpillar Locomotion. *IEEE/ASME Trans. Mechatronics* **2016**, *21*, 1702–1710. [CrossRef]
12. Jang, Y.; Nabae, H.; Endo, G.; Suzumori, K. Analysis of the multi-balloon dielectric elastomer actuator for traveling wave motion. *Sensors Actuators Phys.* **2022**, *333*, 113243. [CrossRef]
13. Watanabe, M.; Tsukagoshi, H. Flexible Sheet Actuator That Generates Bidirectional Traveling Waves. In Proceedings of the 2018 IEEE/ASME International Conference on Advanced Intelligent Mechatronics (AIM), Auckland, New Zealand, 9–12 July 2018; pp. 328–333.
14. Zhao, T.; Fan, Y.; Lv, J. Photomorphogenesis of Diverse Autonomous Traveling Waves in a Monolithic Soft Artificial Muscle. *ACS Appl. Mater. Interfaces* **2022**, *14*, 23839–23849. [CrossRef]
15. Mansouri, M.; Hsiao-Wecksler, E.T.; Krishnan, G. Toward Design Guidelines for Multidirectional Patient Transfer on a Bed Surface Using Traveling Waves. *J. Mech. Robot.* **2024**, *16*, 074501. [CrossRef]
16. Takeyama, J.; Ichikawa, A.; Hasegawa, A.; Kim, E.; Fukuda, T. A Soft Robot Mimicking snail’s foot. In Proceedings of the 2018 International Symposium on Micro-NanoMechatronics and Human Science (MHS), Nagoya, Japan, 9–12 December 2018; pp. 1–3.
17. Xin, W.; Pan, F.T.; Li, Y.; Chiu, P.W.Y.; Li, Z. A Novel Biomimic Soft Snail Robot Aiming for Gastrointestinal (GI) Tract Inspection. In Proceedings of the 2020 8th IEEE RAS/EMBS International Conference for Biomedical Robotics and Biomechatronics (BioRob), New York, NY, USA, 29 November–1 December 2020; pp. 1049–1054.
18. Zhu, R.; Fan, D.; Wu, W.; He, C.; Xu, G.; Dai, J.S.; Wang, H. Soft Robots for Cluttered Environments Based on Origami Anisotropic Stiffness Structure (OASS) Inspired by Desert Iguana. *Adv. Intell. Syst.* **2023**, *5*, 2200301. [CrossRef]
19. Martinez-Sanchez, D.E.; Sandoval-Castro, X.Y.; Cruz-Santos, N.; Castillo-Castaneda, E.; Ruiz-Torres, M.F.; Laribi, M.A. Soft Robot for Inspection Tasks Inspired on Annelids to Obtain Peristaltic Locomotion. *Machines* **2023**, *11*, 779. [CrossRef]
20. Sun, X.; Nose, A.; Kohsaka, H. A vacuum-actuated soft robot inspired by Drosophila larvae to study kinetics of crawling behaviour. *PLoS ONE* **2023**, *18*, e0283316. [CrossRef]
21. Watanabe, M.; Tsukagoshi, H. Soft sheet actuator generating traveling waves inspired by gastropod’s locomotion. In Proceedings of the 2017 IEEE International Conference on Robotics and Automation (ICRA), Singapore, 29 May–3 June 2017; pp. 602–607.
22. Xu, L.; Chen, H.; Zou, J.; Dong, W.; Gu, G.; Zhu, L.; Zhu, X. Bio-inspired annelid robot: A dielectric elastomer actuated soft robot. *Bioinspir. Biomim.* **2017**, *12*, 025003. [CrossRef] [PubMed]
23. Liu, Z.; Wang, Y.; Wang, J.; Fei, Y. Design and Locomotion Analysis of Modular Soft Robot. *Robotica* **2022**, *40*, 3995–4010. [CrossRef]
24. Zhang, Y.; Yang, D.; Yan, P.; Zhou, P.; Zou, J.; Gu, G. Inchworm Inspired Multimodal Soft Robots With Crawling, Climbing, and Transitioning Locomotion. *IEEE Trans. Robot.* **2022**, *38*, 1806–1819. [CrossRef]
25. Yu, M.; Yang, W.; Yu, Y.; Cheng, X.; Jiao, Z. A Crawling Soft Robot Driven by Pneumatic Foldable Actuators Based on Miura-Ori. *Actuators* **2020**, *9*, 26. [CrossRef]
26. Ge, J.Z.; Calderón, A.A.; Chang, L.; Pérez-Arancibia, N.O. An earthworm-inspired friction-controlled soft robot capable of bidirectional locomotion. *Bioinspir. Biomim.* **2019**, *14*, 036004. [CrossRef]
27. Li, M.; Wang, G.; Wang, J.; Zheng, Y.; Jiao, X. Development of an inchworm-like soft pipe robot for detection. *Int. J. Mech. Sci.* **2023**, *253*, 108392. [CrossRef]
28. Yu, Z.; Peiyu, H.; Bo, Y.; Zhibin, Y.; Dongjie, L.; Guoqi, D. Design and Motion Simulation of a Soft Robot for Crawling in Pipes. *Appl. Bionics Biomech.* **2023**, *2023*, 5334604. [CrossRef]
29. Wan, J.; Sun, L.; Du, T. Design and Applications of Soft Actuators Based on Digital Light Processing (DLP) 3D Printing. *IEEE Access* **2023**, *11*, 86227–86242. [CrossRef]
30. Takayama, T.; Taneda, T. Weaving Method to Avoid Interfere between Inflatable Tubes and Strings for 2D Weaved Tube Plane Surface Soft Actuator. In Proceedings of the 2019 Domestic Conferences of the System Integration (SI) Division, Takamatsu, Japan, 12–14 December 2019; pp. 2888–2889.
31. Sugano, N. Ultrasonic Motor. *J. Horol. Inst. Jpn.* **1988**, *124*, 63–79.

**Disclaimer/Publisher’s Note:** The statements, opinions and data contained in all publications are solely those of the individual author(s) and contributor(s) and not of MDPI and/or the editor(s). MDPI and/or the editor(s) disclaim responsibility for any injury to people or property resulting from any ideas, methods, instructions or products referred to in the content.